Thermodynamic and dynamic fragility in metallic glass-formers

Thermodynamic and dynamic fragility in metallic glass-formers

Giulia Dalla Fontana and Livio Battezzati[1]

Dipartimento di Chimica e Centro NIS,

Università di Torino, Via P. Giuria 7, 10125, Torino, Italy

Abstract:

The paper focuses on the study of glasses using models of thermodynamic and transport properties (e.g. heat capacity, viscosity and liquid fragility) of various alloys in comparison with organic and inorganic substances. The work attempts to identify possible correlations and trends in these properties which can relate to indicators of melt fragility for metallic glasses. The ratio of the specific heat integral between selected temperatures gives only a rough indication of the fragility behaviour. More insight is gained in considering the thermodynamic fragility index derived from the PEL model having either a hyperbolic or Gaussian distribution of energy minima. The Wang-Angell-Richert correlation holds for some metallic glasses. Deviations from it help in identifying hidden transitions in the liquid state.

Keywords: Metallic glasses, specific heat, glass transition, amorphous materials, melt fragility.

1. Introduction:

Metallic glasses are usually obtained by rapid quenching deep eutectics [1]. Thermodynamically this implies liquid stabilization down to the low melting point.

[1] Corresponding Author: e-mail: livio.battezzati@unito.it, tel +390116707567, fax +390116707855.

Rapid quenching suppresses crystal nucleation letting the supercooled liquid survive well below the melting point. Here transport properties are important: the liquid viscosity must become quickly high enough to freeze the structure into a glass.

If we consider, for simplicity, a binary eutectic with no miscibility of components in the solid-state, the melting enthalpy of the eutectic mixture (ΔH_m) is given by the melting enthalpies of the proper amount of individual components at the eutectic temperature plus the effect of mixing the elements in the liquid state, i. e. $\Delta H_{eut} = \Delta H_{elements} + \Delta H_{mix}$ [2]. In metallic glass-formers ΔH_{mix} is definitely negative providing stabilization to the liquid. It is also temperature dependent in that it decreases on decreasing temperature because of the contribution of an excess mixing term to the specific heat of the liquid glass-former being definitely higher than that of the crystal at all temperatures [3]. When vitrification occurs there is a jump in specific heat from the value of the undercooled liquid to that of the glass which is close to that of the crystal phases. Therefore, the liquid specific heat is a relevant parameter for glass-formers influencing extensive thermodynamic quantities, e. g.:

$$\Delta S = \Delta S_m - \int_T^{T_m} \Delta C_p \, d \ln T \qquad (1)$$

with ΔS the difference in entropy, $\Delta S_m = \frac{\Delta H_m}{T_m}$ where ΔH_m is the melting enthalpy, and ΔC_p the difference in specific heat between the liquid, $C_p^{\,l}$, and the solid, $C_p^{\,s}$, and T_m is the melting temperature [4]. Being ΔC_p positive, ΔS decreases with decreasing temperature and should become nil at the so-called Kauzmann temperature (T_k). The material, however, becomes a glass at the glass transition temperature, $T_g > T_k$. It has been debated whether the concept of an entropy catastrophe at T_k is actually acceptable [5], nevertheless T_k is useful as a reference state for the glass.

The rate of entropy loss on undercooling depends on the shape of the specific heat curves of the liquid and of the solid. As a consequence, the specific heat trend should reflect the so-called melt fragility. Angell [6-7] has termed thermodynamic fragility a parameter, m_T, defined as:

$$m_T = \left[\frac{d \frac{\Delta S_g}{\Delta S}}{d \frac{T_g}{T}} \right]_{T=T_g} \qquad (2)$$

Considering the definition of ΔS in eq. (1), it is easily shown that m_T is expressed by the ratio $\Delta C_p(T_g)/\Delta S_g$ where ΔS_g is the entropy difference between liquid and glass at the experimental T_g.

The concept of melt fragility was originally introduced by considering liquid viscosity, η, as a function of temperature with the parameter, m, defined as [6]:

$$m = \left[\frac{d \log(\eta)}{d \frac{T_g}{T}} \right]_{T=Tg} \qquad (3)$$

Glass forming liquids are classified as strong or fragile depending on their viscosity behaviour when approaching the glass transition. In an Arrhenius plot the viscosity of strong liquids has an almost linear trend. On the contrary, the viscosity of fragile liquids shows highly non-Arrhenius behaviour, i. e. they manifest a progressive change in the mobility kinetics [8, 9]. This is expressed by the Adams-Gibbs and Vogel-Fulcher-Tammann (VFT) equations [7]: i. e.

$$\eta = A \exp\left[\frac{C}{TS_c} \right] \qquad (4)$$

where C and A are constants and S_c is the configurational entropy of the liquid providing the link between thermodynamics and kinetics of glass-formers, and

$$\eta = \eta_0 \exp\,[B/(T-T_0)] \qquad (5)$$

where B and η_0 are constants and T_0 is the Vogel's temperature at which viscosity would diverge. The two equations become identical if a hyperbolic behaviour of ΔC_p versus temperature is assumed to calculate S_c. The reference state of the specific heat is usually taken as the specific heat of crystalline phases in view of its closeness to that of the glass and therefore S_c is approximated by ΔS. It follows that T_k and T_0 should coincide. To corroborate this, a correlation between m_T and m [6] has been demonstrated for several substances [2].

Recent application of the Potential Energy Landscape (PEL) model has provided insight into the correlation between thermodynamics and dynamics of glass-forming liquids. In the PEL model the inherent structures of the liquid correspond to energy minima, comprised in different basins, describing its configurational space. The minima are distributed in energy and accessed in large number at high temperature whereas the kinetic arrest at the glass transition relates to the number still accessible at lower temperatures. The thermodynamic properties are related to the average value of the minima in potential energy available at every temperature, while the potential energy topology controls the dynamics [11]. As a consequence of multiple configurations in the PEL there is no single glassy state [12]. The relaxation between different states within a

[2] The Adams-Gibbs model is used here because of the straightforward relationship it expresses between liquid entropy and viscosity. The free volume model is often successfully employed to express viscosity. In the Cohen-Turnbull [9] notation $\eta = A\exp\left[\frac{\gamma v^*}{v_f}\right]$ where γv * is the product of free parameters and v_f is the free volume of the liquid/glass [12]. Note that the free volume approach provides the VFT equation if v_f depends linearly on the temperature.

basin and among various basins is the basis for the dynamics of the liquid as reflected in the viscosity behaviour as a function of temperature.

The PEL statistical thermodynamic model expresses changes in entropy as due to changes in shape of potential energy basins. The enumeration function of the basins, i. e. the energy distribution of the minima in the PEL, has been expressed in different forms to represent the liquid configurational entropy. More common is the Gaussian distribution of energies whereas the shape of the specific heat curve of the liquid as a function of temperature mentioned above, has suggested an hyperbolic distribution. Expressions of fragility parameters have been derived from these distributions as a function of thermal parameters T_k and T_g [7].

This paper seeks to apply the above concepts to metallic glass formers by deriving thermodynamic fragility parameters and compare them with kinetic ones available in the literature as well as to compare the fragility of metallic and non-metallic glass-formers. The paper is organized as follows: expressions of the liquid specific heat in the range from T_k to well above T_m are used to derive fragility indicators being solely function of significant temperatures, the thermodynamic data of the literature are critically reviewed and employed to test both thermodynamic and kinetic fragility indexes, the test is then extended to non-metallic glass formers to derive comparative conclusions.

2. The liquid specific heat in metallic glass-formers

The evolution of the specific heat of the liquid as a function of temperature is expected to reflect the fragile/strong behaviour of the melt. Fig. 1 reports the specific heat of liquid (C_p^l) and crystal phases (C_p^s) as derived from experimental data of $Pd_{40}Ni_{40}P_{20}$ [13]. The relevant temperatures T_m, T_g, and T_k, of the alloy are marked.

The areas of the rectangles in the graph match the integral of the specific heat difference between two relevant temperatures, i. e. they express the average values of ΔC_p between T_k and T_g and between T_g and T_m ($\overline{\Delta C_p}'$ and $\overline{\Delta C_p}''$ respectively). The ratio of C_p^l to C_p^s or the jump in specific heat at T_g have been proposed as a metric for the fragility showing diverse behaviour for different classes of materials, i. e. organic, inorganic, polymeric substances [14]. We pose the question whether amorphous alloys can be ranked according to the above average values and the related temperatures.

The specific heat of molten glass-formers has been described with T^{-n} functions, $\Delta C_p(T) = \frac{k}{T^n}$ where k is a material specific constant and n is a value between 0 and 2 [6]. We then begin by assuming a hyperbolic trend for ΔC_p of the alloy. Consequently, we obtain:

$$\int_{T_1}^{T_2} \frac{A}{T} dT = A \ln \frac{T_2}{T_1} = (T_2 - T_1)\overline{\Delta C_p} \qquad (6)$$

$$\overline{\Delta C_p} = \frac{A}{T_2 - T_1} \ln \frac{T_2}{T_1} \qquad (7)$$

where $\overline{\Delta C_p}$ is the average value between two selected temperatures. From Fig. 1. it is deduced that $\overline{\Delta C_p}' > \overline{\Delta C_p}''$. The ratio between the average values, i. e.

$$\frac{\overline{\Delta C_p}''}{\overline{\Delta C_p}'} = \frac{T_g - T_k}{T_m - T_g} \frac{\ln \frac{T_m}{T_g}}{\ln \frac{T_g}{T_k}} \qquad (8)$$

depends only on the relevant temperatures and could possibly reflect the fragility of the alloy.

Using a T^2 function, the above ratio becomes:

$$\frac{\overline{\Delta C_p}''}{\overline{\Delta C_p}'} = \frac{T_k}{T_m} \qquad (9).$$

On the right hand side of eq. (9) the information on the intermediate temperature between T_m and T_k is lost. With the assumption of a T^{-2} dependence of ΔC_p, the ratio of two significant temperatures expresses the trend of the specific heat curve although with less experimental base than before. In this respect, it is worth remembering that one of the most used empirical indexes of glass formability is T_g/T_m [2] to which the present discussion provides a thermodynamic background.

3. Critical analysis of literature data

Data on transition temperatures for many amorphous alloys are available in the literature whereas specific heat data are scarce and subject to considerable error. The main sources of scatter will be summarized in the following to motivate the critical selection among available data which has been performed for the present analysis. The metallic glasses that have been considered are alloys based on Zr, La, Pd, Cu, Mg, Au and Pt. The relevant compositions and data are reported in Tab. 1

The specific heats are obtained from enthalpy data using suitable functions [15]: $C_p^s = 3R + a\,T + bT^2$ and $C_p^l = 3R + c\,T + dT^{-2}$ where $R = 8{,}3142\ Jmol^{-1}K^{-1}$, while *a*, *b*, *c*, and d are fitting parameters. In some articles, the data are expressed in simplified form, e. g. with a linear dependence on temperature [4] because of the few experimental points available. These have not been used here. Care has been taken that the specific heat of the undercooled liquid state in the temperature range between the glass transition and the crystallization of the glass is described correctly. This refers to data obtained by DSC in the continuous heating mode and implies that such range be substantial so that the heat effect due to relaxation at T_g is completed, thus avoiding spurious contribution to the excess specific heat.

Since in most cases it is necessary to interpolate the liquid specific heat in the range from the crystallization temperature to the melting point of the alloy, the fitting function

should not give unphysical minima or maxima. Clearly, should a true transition occur in the liquid within such temperature range, it will not be detected.

A fortiori, the above warning applies to extrapolating functions to obtain the Kauzmann temperature. An estimate of the uncertainty on it for alloys of Tab. 1 has been obtained by using eq. (2) together with T^n ($0<n<2$) expressions of ΔC_p and deviations of experimental variables. The estimated error is in excess of 50 K in all cases, similarly to data on inorganic and organic glasses [7]. Analogously, the uncertainty on T_0 values has been evaluated from the VFT expression resulting of the order of 10-40 K according to the amount of deviation of viscosity in the temperature range above T_g.

Whenever possible, i. e. when the enthalpies of crystallization, ΔH_x, were provided in the papers, the internal consistency of the set of data was checked using eq. (1). In fact, metastable phases may persist in the alloy up to the melting point. Should this occur, the heat of fusion will be underestimated.

It is also known that T_g shifts as a function of heating rate [16], so the data used in this work refer to a limited range of heating rates commonly used in the literature (10 to 40 $Kmin^{-1}$). Finally, data obtained in different laboratories were used for comparison, when available.

4. Models and analyses of thermodynamic and transport properties.

Fig. 2 reports the function derived by modelling ΔC_p as hyperbolic, versus the ratio of the average values of ΔC_p between T_m, T_g, and T_k calculated from the experimental data on metallic glasses and on various organic and inorganic substances reported in the literature.

The specific heat difference for a group of substances can actually be represented by the hyperbolic trend within the data scatter, the largest deviation for alloys is shown by the

Pt-based glasses and by some of the Zr-based ones. The ordinate of all Zr-based alloys is almost the same, while there is a large scatter on the horizontal axis. Also the points relating to $Mg_{65}Cu_{25}Y_{10}$, coming from different references in the literature, are shifted on the horizontal axis. This is an indication of the level of uncertainty associated with experimental data.

Fig. 3 reports the function derived by modelling ΔC_p as T^{-2}, versus the ratio of the average values of ΔC_p between T_m, T_g, and T_k calculated from the experimental data. Here, the Pd- and Pt-based alloys fit the expected trend whereas a large number of the other substances display diverse behaviour. Overall, the points representative of alloys are better fitted by the T^{-1} function than the T^{-2} one.

Since T_k is obtained by extrapolation of ΔC_p data, the ordinates of Figs 2 and 3 are partially obtained from the same quantities from which the abscissa are derived. Therefore, T_0 which is derived from viscosity measurements has been employed instead of T_k in an alternative plot to Fig. 2. Although there are changes in the position of individual points (Fig. 4), the overall trend is not modified suggesting that the two temperatures can be considered as equivalent in describing the melt fragility within the limits of the present approach. We do not enter here the debate on whether T_k and T_0 actually coincide or should be clearly distinguished (as claimed for instance by Tanaka [28]) also in view of the deviation of both of them which has been stated in the previous paragraph.

The analysis performed so far shows that parameters derived from the specific heat function can provide only a very rough indication of the fragility behaviour of the liquid. This is due both to the simplified models needed to express the parameters and to the experimental uncertainty.

Turning now to more common parameters expressing the thermodynamic fragility, the entropy derivative in eq. (4) has been shown to be equivalent to the ratio of $\Delta C_p(T_g)$ to ΔS_g, where ΔS_g is the residual entropy at T_g [7].

The thermodynamic and kinetic fragilities have been correlated [7] by employing the kinetic definition of Speedy:

$$m_s = \frac{d\left[\frac{\log(\eta(T)/\eta_\infty}{\log(\eta(T_g)/\eta_\infty}\right]}{d(T_g/T)} = \frac{m}{17} \qquad (10)$$

The factor 17 refers to the decimal logarithmic range of viscosity spanned from the high temperature limit ($\eta \approx 10^{-5}$ *Pa·s*) to the conventional value of $\eta = 10^{12}$ at the glass transition.

Assuming an hyperbolic distribution of energy minima in the PEL in association with the Adam-Gibbs expression of viscosity, eq. (4), it turned out that

$$m_T = m_s - 1 = \frac{T_K}{T_g - T_K} \qquad (11).$$

To verify the correlation of thermodynamic parameters for fragility and that based on the viscosity, we have plotted the *m* obtained from experimental viscosity data versus m_T from eq (11). In dynamic DSC experiments, however, the viscosity of the melt in correspondence of the temperature range where the glass transition is detected is lower than the conventional value, typically of two order of magnitude [16]. Therefore, we allow for a range of m_s values from *m/17* to *m/15*.

The correlation for metallic amorphous alloys looks poor such as those shown in Figs. 2 and 3.[3] However, to put it in the proper perspective, the insert shows the same plot for

[3] Note that the parameter m_T can be related to the T_k/T_m quantity of eq. (9) as $\frac{1}{m_T} - 1 = q\frac{T_k}{T_m}$.

various glass forming substances where a correlation is recognized. The deviation from the expected trend for several organic and inorganic compounds is of the same order as for metallic glasses. Furthermore, in both cases a few points are clearly displaced at high values of m_T indicating either an inherent discrepancy between the two indexes or that the data used to compute them contain a fault, most likely the thermodynamic ones. This is suggested by considering the analogous plot shown in Fig. 6 where T_0 has been substituted for T_k and most points are much closer to the correlation line.

Assuming a Gaussian distribution of energy minima in the PEL in association with the Adam-Gibbs expression of viscosity, eq. (4) [7], the m_T becomes

$$m_T = m_S - 1 = \frac{2T_k^2}{T_g^2 - T_k^2} \qquad (12).$$

A comprehensive plot including the correlations expressed by eqs. (11) and (12) is shown in Fig. 7. Inspection of Fig. 7 provides further confirmation that metallic glasses conform to the general trend of glass formers and that all metallic glass formers classify among fragile-intermediate melts. The overall correlation for metallic glasses seems more satisfactory when employing eq. (12), however, the correlation curves are very close and, as already suggested for conventional glass-formers [7], we are not in the position of expressing a favour for either distributions also in view of the scatter displayed by several points. The correlation is improved by using T_0 instead of T_k as already shown in Fig. 6 for both distributions.

We consider finally the strong correlation found by Wang, Angell and Richert between m (obtained experimentally from viscosity) and m_{calc}, obtained from their formula containing thermodynamic quantities and the glass transition temperature [6]

---

by using $q=T_g/T_m$. The ratio q varies in the 0.5-0.75 range for all glass-formers therefore the above relation is only indicative and it is expected that m_T be a better metric for fragility than T_k/T_m.

$m_{calc}=56T_g\Delta C_p(T_g)/\Delta H_m$ (13).

Of the many compounds for which data are known, only a few deviate from the correlation shown in the insert of Fig. 8. Fig. 8 show the same plot for metallic glasses. Again the scatter is large for most of them, whereas some follow the general trend within the computed uncertainty. Note that the points displaying the larger scatter are the same which fell wide off the correlation line in Fig. 5.

Analysing the data of the insert, Angell suggested reasons for the deviation of some points such as the ring-chain equilibrium of Se near T_g and the effect of decaline being a *cis-trans* mixture. These influence either the thermodynamic or kinetic behaviour of the melt [6]. Similarly, a ring-chain equilibrium in the liquid state of sulphur, causes overlap of relaxation effects affecting the kinetic fragility of the melt with large deviation in the *m* index [29].

Following up this line of thought, the points referring to the metallic glasses which mostly deviate from the Angell's relation, should be explained by modifications of interactions in the liquid state [13]; however, until now there is no clear experimental confirmation of this in the literature. While it has been verified in several instances that the experimental C_p^s for metallic glasses are close to those obtained by the Neumann-Kopp's law of mixtures, the liquid C_p^l are peculiar for alloys and reflect the chemical interactions in mixing which may change as a function of temperature. A neat example is provided by the $Te_{80}Ge_{20}$ alloy which is a metallic liquid above the melting point becoming a semiconductor in the undercooling regime. This transition gives rise to a peak in the specific heat of the liquid in between the melting point and the glass transition [30]. Clearly, the two difference quantities appearing in formula (13) refer to phases having different structure, i. e. a semiconducting liquid and the glass in the case of $\Delta C_p(T_g)$, and a metallic liquid and crystal phases in the case of ΔH_m . Therefore, eq (13) becomes devoid of significance. Actually, using the data in [30] to evaluate the

kinetic *m* from the relative width of the temperature range of glass transition according to the Moyhnian method [31], the value of 44 is obtained which differs significantly from the 65 value of the computed m_{calc}.

A second case enforces this discussion. From viscosity data of the $Au_{77}Ge_{13.6}Si_{19.4}$ glass-forming melt, the kinetic *m* was obtained in the 80 to 85 range [32]. Applying the formula (13), m_{calc} turns out to be 40. Here the discrepancy occurs because of posing the crystalline state as reference. The equilibrium state for the $Au_{77}Ge_{13.6}Si_{19.4}$ metallic glass is a mixture of fcc Au and semiconducting Si-Ge solid solution [33] whereas the liquid and glassy phases are metallic in character. The ΔH_m of the alloy is, therefore, much influenced by the high heat of fusion of the semiconductor phase. The related, although better glass-former, $Au_{49}Cu_{26.9}Ag_{5.5}Pd_{2.3}Si_{16.3}$ metallic glass crystallizes almost entirely into metallic phases, a solid solution and three silicides [34]. The kinetic *m* obtained with the Moyhnian method is 45 and m_{calc} is of the order of 53.

It should finally be noted that fragile-to-strong transitions have been derived in computer studies of the PEL of liquid silica as a function of pressure leading to polyamorphism and peaks in the isochoric specific heat curves [35]. This concept has been generalized to various classes of glass-formers displaying increasing intermediate order by proposing that the location of the specific heat peak changes very substantially from well above the melting point in very strong melts, e. g. silica, to below the glass transition in fragile ones, e. g. organic substances [12]. Metallic glasses have not been considered to date in this picture, although a fragile-to strong transition has been inferred from the hysteretic behaviour of viscosity on heating and cooling the bulk glass-former $Zr_{41.2}Ti_{13.8}Cu_{12.5}Ni_{10.0}Be_{22.5}$ between 907 K and 1300 K, and attributed to the destruction of medium- and short-range order in the liquid state [36]. A volume transition has been recently revealed by containerless undercooling similar melts using electrostatic levitation [37]. Clearly, careful determination of properties in alloys

forming metallic glasses can give more insight on kinetic and thermodynamic fragility. It is apparent that there cannot be a universal index of fragility. It must be recognized that they help in pointing out discrepancies in either the quality of data or the actual occurrence of structure modifications in the melt.

5. Conclusions

In this paper, attention has been focussed on the study of the thermodynamic and dynamic properties of glass-forming metallic melts in constant comparison to organic and inorganic substances. We started by considering the specific heat capacity of the melt as the parameter that links the various thermodynamic quantities, attempting to correlate it to the fragility of the melt. In this respect, taking ΔC_p proportional to $1/T^n$, functions of the relevant temperatures of the glass (T_m, T_g, T_k and T_0) have been derived to verify such possible correlation. The points representative of alloys are better fitted by the T^{-1} function than the T^{-2} one. However, these provide only a very rough indication of the fragility behaviour of the liquid also in view of the experimental uncertainty which has been carefully evaluated for all metallic glasses by means of a critical assessment of literature data.

The kinetic index m of fragility has been considered versus the thermodynamic one m_T for metallic glasses by applying expressions derived from the PEL model assuming both a hyperbolic and a Gaussian distribution of energy minima. The two quantities correlated for all substances. For metallic glasses the correlation is more satisfactory if T_0 instead of T_k is employed. Overall, metallic glasses classify among fragile-intermediate melts.

The Wang-Angell-Richert relationship (eq. 13) developed to compute m for organic and inorganic substances, was shown to hold for some metallic glasses. Deviation from it for other melts could be explained with hidden transitions in the undercooled regime and

variations in bonding (e. g. semiconducting in crystal and metallic in glass) providing suggestion for *ad hoc* experiments to verify them.

Acknowledgements

Work performed for “Progetto di Rilevante Interesse Nazionale, PRIN 2008” and the “Thermolab” ESA-MAP Project. Fondazione S. Paolo is acknowledged for support to CdE NIS. GDF wishes to acknowledge the support of a PhD grant from Fondazione CRT.

References

[1] Wang WH, Dong C, Shek CH. Mat Sci Eng R 2004;44:45.
[2] Battezzati L, Greer AL. Int J Rapid Solidif 1987;3:23.
[3] Battezzati L. Metallic glasses. In: Lechter TM, editor. Chemical Thermodynamics IUPAC "Chemistry for the 21st Century" monograph. Oxford: Blackwell Science, 1999. p.239.
[4] Cai A, Xiong X, Liu Y, Chen H, An W, Li X, Zhou Y, Luo Y. Eur Phys J B 2008;64:147.
[5] Stillinger FH, Debenedetti PG, Truskett TM. J Phys Chem B 2001;105:11809.
[6] Wang LM, Angell CS, Ranko R. J Chem Phys 2006;125:074505.
[7] Ruocco G, Sciortino F, Zamponi F, De Michele C, Scopigno T. J Chem Phys 2004;120:10666.
[8] Fan GJ, Choo H, Liaw PK. J Non-Cryst Solids 2005;351:3879.
[9] Busch R. J Miner Met Mater Soc 2000;52:39.
[10] van den Beukel A, Sietsma J. Acta Metall Mater 1990;38:383.
[11] Hu L, Bian X, Wang WH, Liu G, Jia Y. J Phys Chem B 2005;109:13737.
[12] Angell CA. Mrs Bull 2008;33:1.
[13] Gallino I, Schroers J, Busch R. J Appl Phys 2010;108:063501.
[14] Huang DM, Gregory B. J Chem Phys 2001;114:5621.
[15] Jiang QK, Wang XD, Nie XP, Zhang GQ, Ma H, Fecht HJ, Bendnarcik J, Franz H, Liu YG, Cao QP, Jiang JZ. Acta Mater 2008;56:1785.
[16] Battezzati L, Castellero A, Rizzi P. J Non-Cryst Solids 2007;353:3318.
[17] Battezzati L. Rev Adv Mater Sci 2008;18:184.
[18] Glade SC, Busch R, Lee DS, Johnson WL, Wunderlich RK, Fecht HJ. J Appl Phys 2000;87:pp. 7242.
[19] Evenson Z, Busch R. Acta Mater 2011;59:4404.
[20] Lu ZP, Li Y, Liu CT. J Appl Phys 2003;93:286.
[21] Senkov ON. Phys Rev B 2007;76:104202.
[22] Jiang QK, Zhang GQ, Yang L, Wang XD, Saksl K, Franz H, Wunderlich R, Fecht H, Jiang JZ. Acta Mater 2007;55:4409.
[23] Ikeda M, Aniya M. Intermetallics 2010;18:1796.
[24] Busch R, Liu W, Johnson WL. J Appl Phys 1998;83:4134.
[25] Fiore G, Battezzati L. J Alloy Compd 2009;483:54.

[26] Legg BA, Schroers J, Busch R. Acta Mater 2007;55:1109.
[27] Mishra R, Dubey K. J Therm Anal Calorim 1997;50:843.
[28] Tanaka H. Phys Rev Lett 2003;90:055701.
[29] Ruta B, Monaco G, Giordano V, Scarponi F, Fioretto D, Ruocco G, Andrikopoulos K, Yannopoulos S. J Phys Chem B 2011;115:14052.
[30] Battezzati L, Greer AL. J Mater Res 1988;3:570.
[31] Moyhnian C. J Am Ceram Soc 1993;76:1081.
[32] Perera DN. J Phys: Condens Matter 1999;11:3807.
[33] Chen HS, Turnbull D. J Chem Phys 1968;48:2560.
[34] Fiore G, Rizzi P, Battezzati L. J Alloy Compd 2011;509, Supplement 1:S166.
[35] Saika-Voivod I, Sciortino F, Poole PH. Nature 2001;412:514.
[36] Way C, Wadhwa P, Busch R. Acta Mater 2007;55:2977.
[37] Li JJZ, Rhim WK, Kim CP, Samwer K, Johnson WL. Acta Mater 2011;59:2166.
[38] Shadrack Jabes B, Agarwal M, Chakravarty C. J Chem Phys 2010;132:234507.
[39] Richet P. Phys Chem Miner 1990;17:79.
[40] Angell CA. J Res Natl Inst Stan 1997;102.
[41] Gordon JM, Rouse GB, Gibbs JH, Risen WM, Jr. J Chem Phys 1976;66:4971.
[42] Carlson HG, Westrum EF. J Chem Phys 1971;54:1464.
[43] Moynihan CT, Angell CA. J Non-Cryst Solids 2000;274:131.
[44] Angell CA, Williams E, Rao KJ, Tucker JC. J Phys Chem 1977;81:238.
[45] Nikolova D, Maneva M. J Therm Anal 1995;44:869.
[46] Richet P, Bottinga Y, Denielou L, Petitet JP, Tequi C. Geochim Cosmochim Ac 1982;46:2639.

Figure Captions

Fig. 1. The specific heat of liquid and crystal phases of a glass-forming alloy and a representation of the integral between selected temperatures.

Fig. 2. Plot of the function of ΔC_p proportional to T^{1} versus the ratio of the average values of ΔC_p at T_m, T_g, T_k. Errors bars are computed from typical available uncertainty of experimental quantities. For simplicity, in this and the following graphs each alloy listed in Tab. 1 will be identified only by means of number in parenthesis, while the organic and inorganic substances are not labelled and are used as [6] and can be identified in this article (see supplementary information online).

Fig. 3. Plot of the function of ΔC_p proportional to T^{-2} versus the ratio of the average values of ΔC_p at T_m, T_g, T_k. Errors bars are computed from typical available uncertainty of experimental quantities.

Fig. 4. Plot of the function of ΔC_p proportional to T^{-2} versus the ratio of the average values of ΔC_p at T_m, T_g, T_0. Errors bars are computed from typical available uncertainty of experimental quantities.

Fig. 5. Plot of the kinetic index m versus the thermodynamic m_T for metallic glasses. The black and red dashed lines refer to the expected linear relationship between m_S and m: $m_S = m/17$ or $m/15$ respectively. The insert reports the same plot for the organic and inorganic glass formers (see supplementary information online).

Fig. 6. Same as Fig. 5 but here T_0 has been substituted for T_k. The insert reports the same plot for the organic and inorganic glass formers (see supplementary information online).

Fig. 7. Plot of the kinetic index m versus the T_g/T_k ratio for metallic, organic and inorganic formers glasses (see supplementary information online). The lines refer to the trend expressed by eqs. 11 and 12. The insert reports the same plot but here T_0 has been substituted for T_k .

Fig. 8. Plot of the calculated m_{calc} from Angell with the measured m fragility index for metallic glasses. The insert reports the same plot for the organic and inorganic glass formers (see supplementary information online).

Tab. 1. Experimental data employed in this paper to compute quantities expressing liquid fragility.

Supplementary information online.

Tab. 1: The formula for the specific heat capacity of liquid and solid alloys and the corresponding references

Tab. 2: List of organic and inorganic substances from Ref [6] and corresponding references. The numbers are same as in [6].

Tab. 1.

	Alloys	T_m[k]	T_g[k]	T_k[k]	T_0[k]	ΔH_m [kJ/mol]	$\Delta C_p(T_g)$ [J/mol·K]	m	Refs.
(1)	$Zr_{46}(Cu_{4.5/5.5}Ag_{1/5.5})_{46}Al_8$	1063	703	671	578	7,104	17,87	49	[15]
(2)	$Zr_{46}Cu_{46}Al_8$	979	715	596	588	8,035	16,41	43	[15]
(3)	$Zr_{41,2}Ti_{13,8}Cu_{12,5}Ni_{10}Be_{22,5}$	937	620	560	412	8,2	22,47	48	[4, 13, 16-17]
(4)	$Zr_{52,5}Cu_{17,9}Ni_{14,6}Al_{10}Ti_5$	1072	675	638		8,2	19,83		[4, 18]
(5)	$Zr_{57}Cu_{15,4}Ni_{12,6}Al_{10}Nb_5$	1091	682	664		9,4	20,82		[4, 18]
(6)	$Zr_{44}Ti_{11}Ni_{10}Cu_{10}Be_{25}$	921	620	504,5	366,6	9,3	19.99	39	[19]
(7)	$La_{55}Al_{25}Cu_{10}Ni_5Co_5$	661	466	363	241,2	6,09	16,05	37	[4, 20-21]
(8)	$La_{55}Al_{25}Cu_{10}Ni_{10}$	662	467	332	254,7	6,84	14,77	35	[4, 20-21]
(9)	$La_{62}Al_{14}Cu_{20}Ag_4$	656	404	314	371	6,118	13,16		[22]
(10)	$Cu_{47}Ti_{34}Zr_{11}Ni_8$	1114	673	537	500	11,3	14,26	59	[4, 13, 16 , 17-19, 23]
(10)	$Cu_{47}Ti_{34}Zr_{11}Ni_8$	1114	673	537	500	11,3	15,47	59	[4, 13, 16-18, 23]
(11)	$Mg_{65}Cu_{25}Y_{10}$	730	411	320	261	8,65	14,63	45	[4, 13, 16-17, 24]
(11)	$Mg_{65}Cu_{25}Y_{10}$	730	411	320	261	8,65	16,13	45	[4, 13, 16-17, 24]
(12)	$Pd_{40}Ni_{40}P_{20}$	884	570	487	396	9,39	19,78	46	[4, 13, 16-17]
(13)	$Pd_{40}Ni_{10}Cu_{30}P_{20}$	798	578	497	418	6,82	21,34	63	[4, 13, 16]
(14)	$Pd_{43}Ni_{10}Cu_{27}P_{20}$	818	582	532	446	5,02	18,73	65	[13, 16-17]
(15)	$Pd_{77,5}Cu_6Si_{16,5}$	1015	628	560	505	7,81	14,09	65	[16, 25]
(16)	$Pt_{57,3}Cu_{14,6}Ni_{5,3}P_{22,8}$	754	480	396	336	11,4	27,86		[13, 26]
(16)	$Pt_{57,3}Cu_{14,6}Ni_{5,3}P_{22,8}$	775	480	396	336	11,4	27,10		[13, 26]

(17)	$Au_{81,4}Si_{18,6}$	636	290	202		9,845	15,80		[27]
(18)	$Au_{77}Ge_{13,6}Si_{9,4}$	625	294	199	241,3	10,627	16,93	85	[8, 10, 27]

Fig. 1.

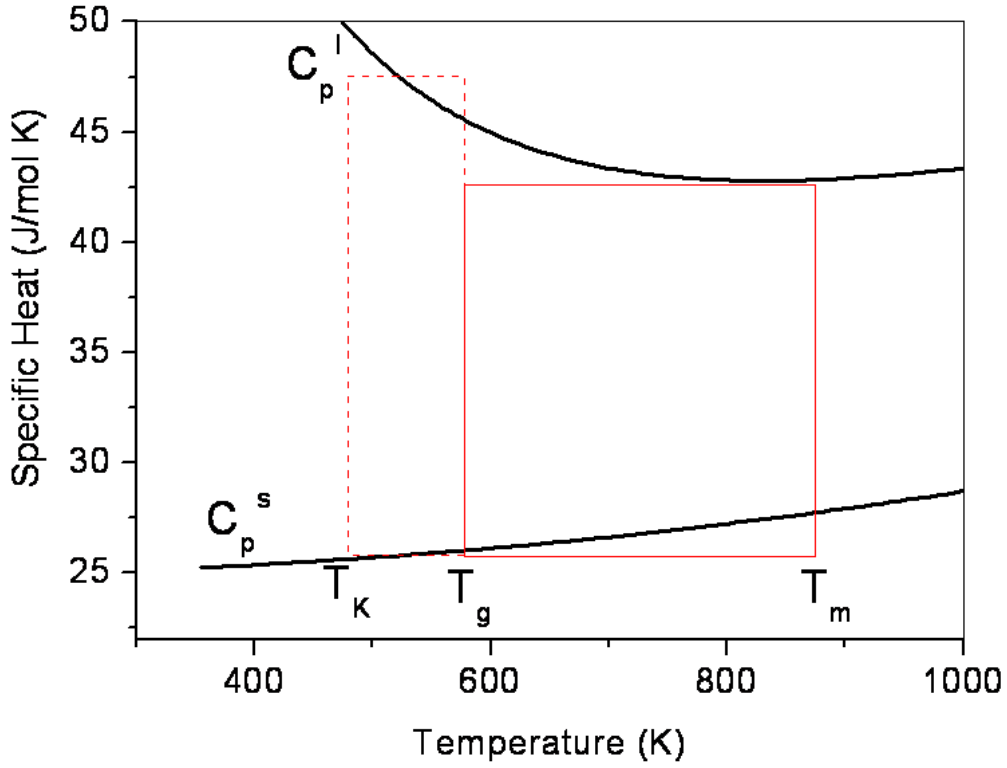

Fig. 2.

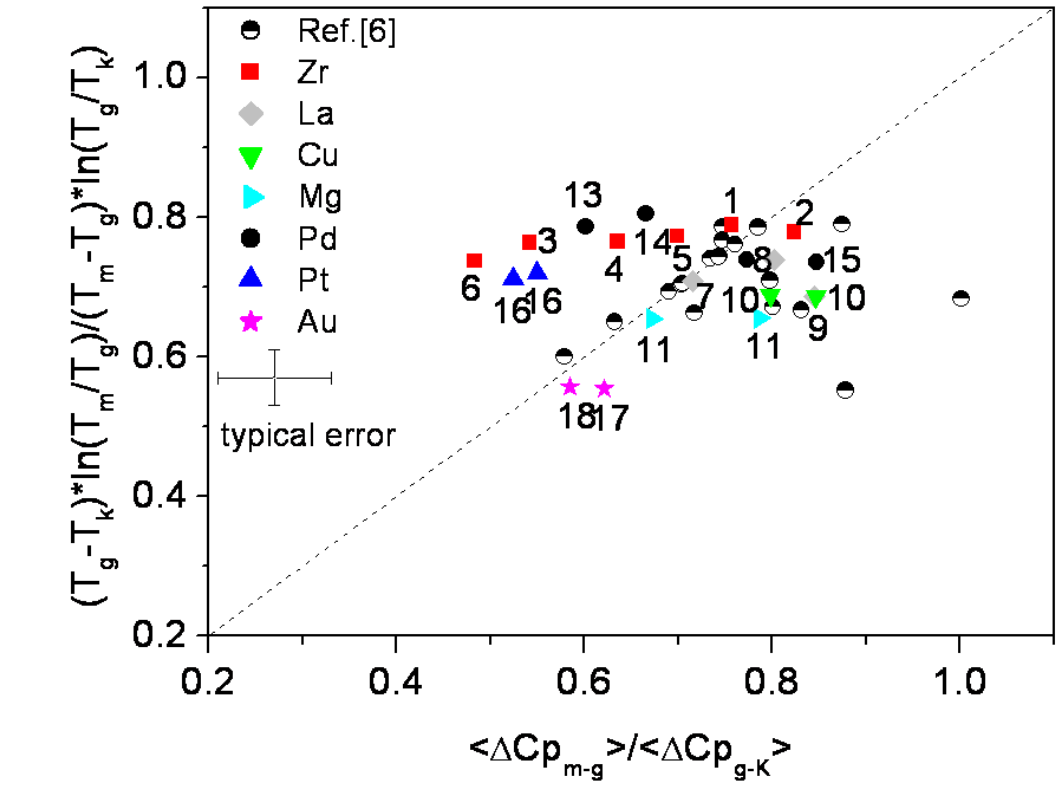
Ref.[6]
Zr
La
Cu
Mg
Pd
Pt
Au
typical error
$(T_g-T_k)*\ln(T_m/T_g)/(T_m-T_g)*\ln(T_g/T_k)$
$<\Delta Cp_{m-g}>/<\Delta Cp_{g-K}>$

Fig. 3.

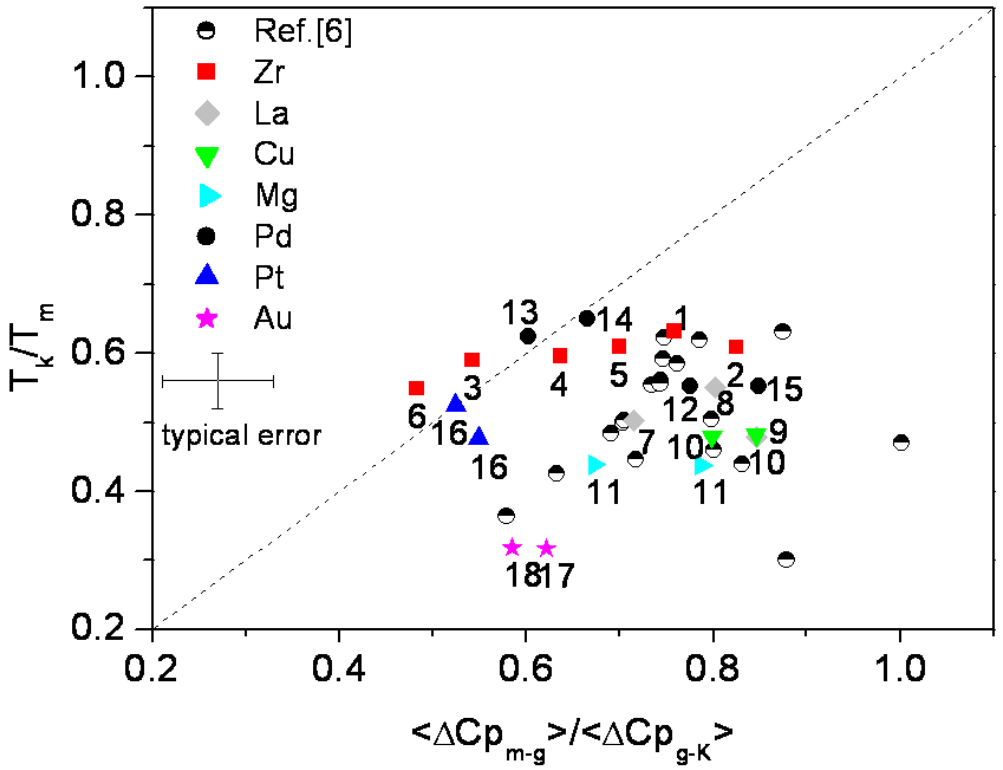
Ref.[6]
Zr
La
Cu
Mg
Pd
Pt
Au
typical error
T_k/T_m
$<\Delta Cp_{m-g}>/<\Delta Cp_{g-K}>$

Fig. 4.

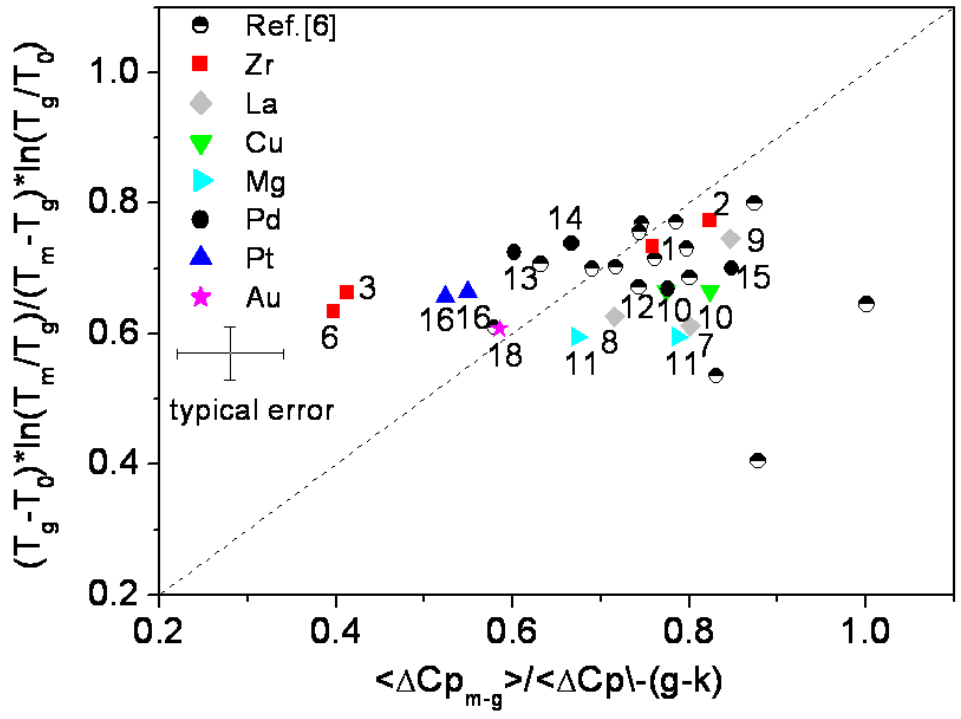
Ref.[6]
Zr
La
Cu
Mg
Pd
Pt
Au
typical error
(T_g-T_0)*ln(T_m/T_g)/(T_m-T_g)*ln(T_g/T_0)
<ΔCp_m-g>/<ΔCp\-(g-k)

Fig. 5.

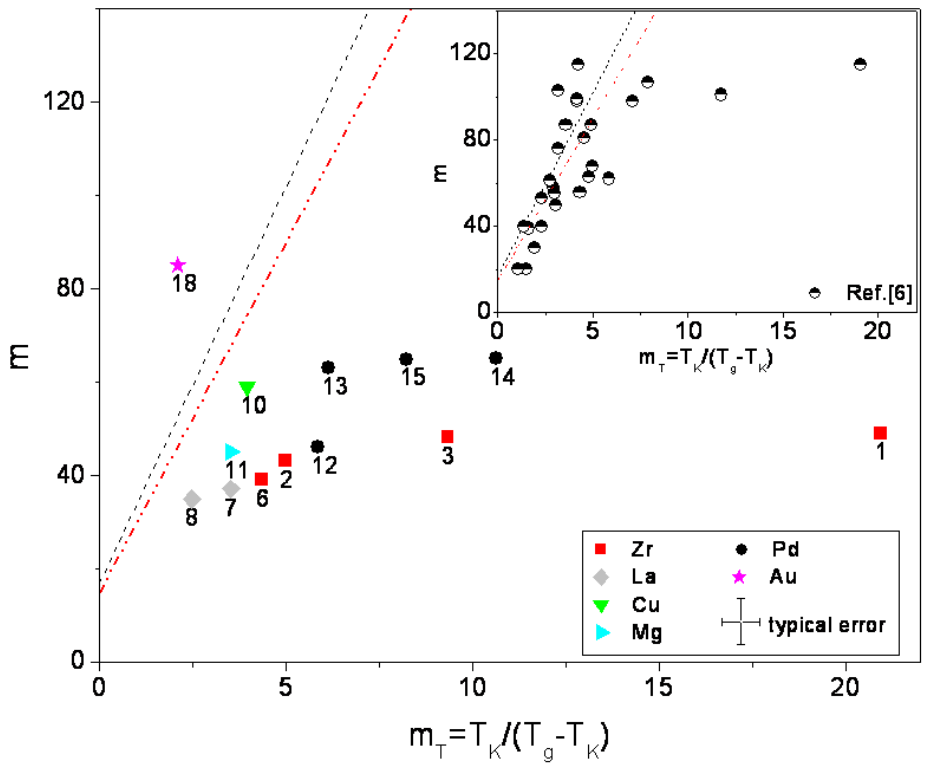
m
m_T=T_K/(T_g-T_K)
Ref.[6]
Zr
La
Cu
Mg
Pd
Au
typical error

Fig. 6.

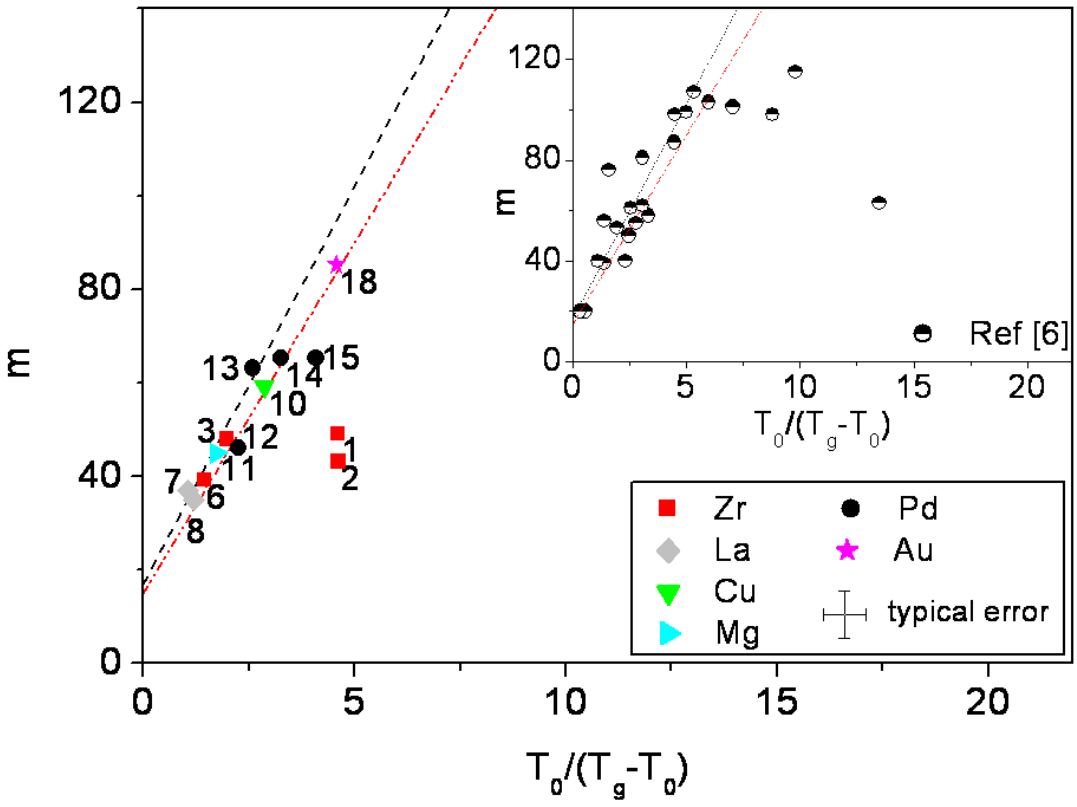
m
$T_0/(T_g-T_0)$
Ref [6]
Zr
La
Cu
Mg
Pd
Au
typical error

Fig. 7.

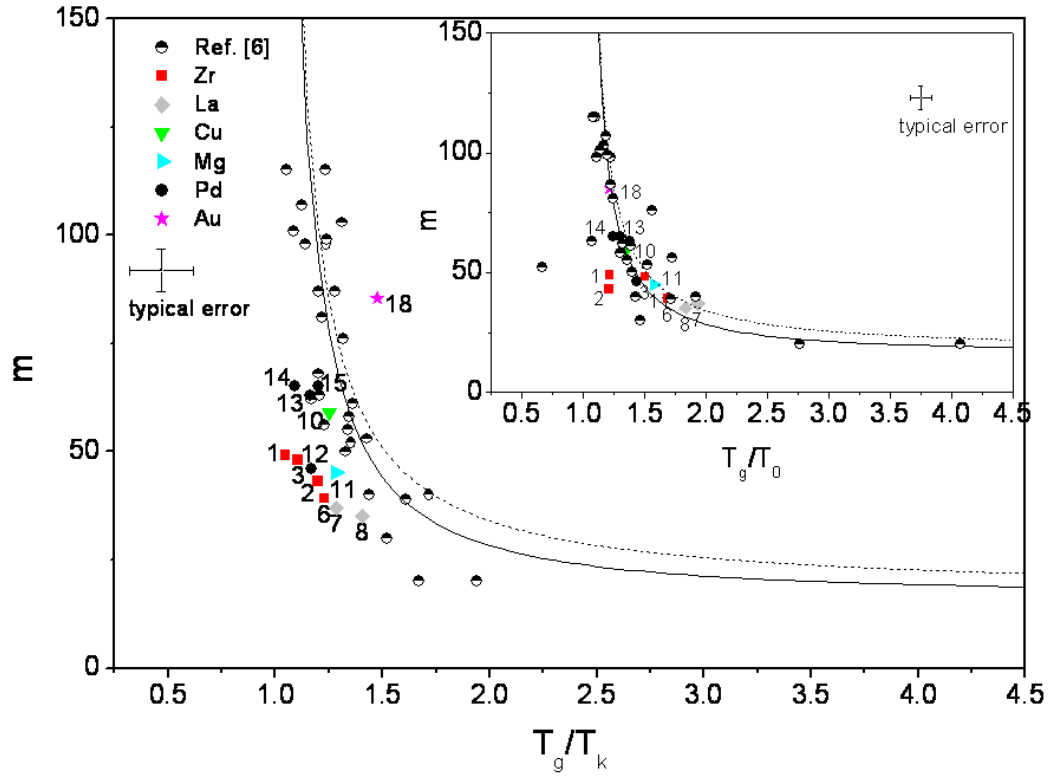
m
T_g/T_k
T_g/T_0
Ref. [6]
Zr
La
Cu
Mg
Pd
Au
typical error

Fig. 8.

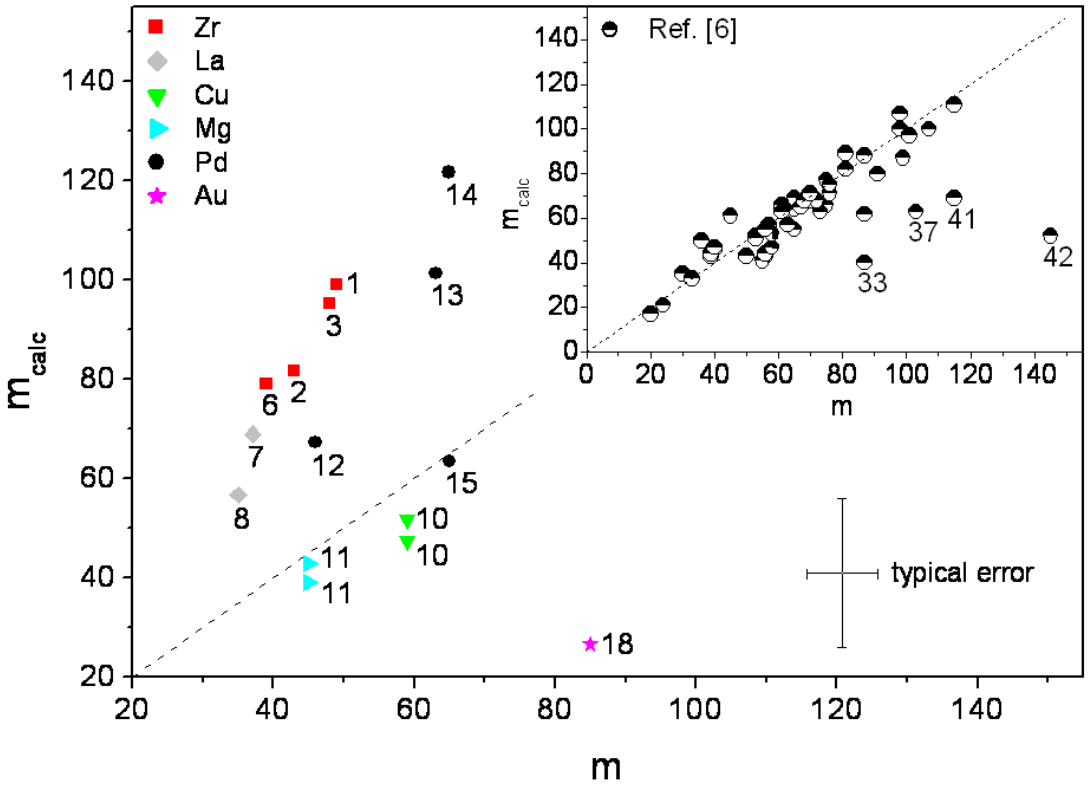

Supplementary information

Tab. 1

	Alloys	C_p [J/mol K]	Refs.
(1)	$Zr_{46}(Cu_{4.5/5.5}Ag_{1/5.5})_{46}Al_8$	$C_p^{\,s} = 3 \cdot 8{,}3142 + (-0{,}000504) \cdot T + 8{,}0089 \cdot 10^{-6} \cdot T^2$ $C_p^{\,l} = 3 \cdot 8{,}3142 + 0{,}01348 \cdot T + 5{,}931 \cdot 10^{6} \cdot T^{-2}$	[15]
(2)	$Zr_{46}Cu_{46}Al_8$	$C_p^{\,s} = 3 \cdot 8{,}3142 + (-0{,}00166) \cdot T + 5{,}59 \cdot 10^{-6} \cdot T^2$ $C_p^{\,l} = 3 \cdot 8{,}3142 + 0{,}01268 \cdot T + 4{,}6084 \cdot 10^{6} \cdot T^{-2}$	[15]
(3)	$Zr_{41,2}Ti_{13,8}Cu_{12,5}Ni_{10}Be_{22,5}$	$C_p^{\,s} = 3 \cdot 8{,}3142 + (-0.008597) \cdot T + 21{,}611 \cdot 10^{-6} \cdot T^2$ $C_p^{\,l} = 3 \cdot 8{,}3142 + 0{,}0092197 \cdot T + 7{,}5841 \cdot 10^{6} \cdot T^{-2}$	[13]
(4)	$Zr_{52,5}Cu_{17,9}Ni_{14,6}Al_{10}Ti_5$	$C_p^{\,s} = 3 \cdot 8{,}3142 + (-0.00861) \cdot T + 16{,}8 \cdot 10^{-6} \cdot T^2$	[18]

		$C_p^{\,l} = 3 \cdot 8{,}3142 + 0{,}0112 \cdot T + 6{,}43 \cdot 10^{6} \cdot T^{-2}$	
(5)	$Zr_{57}Cu_{15,4}Ni_{12,6}Al_{10}Nb_5$	$C_p^{\,s} = 3 \cdot 8{,}3142 + (-0.00302) \cdot T + 8{,}37 \cdot 10^{-6} \cdot T^{2}$ $C_p^{\,l} = 3 \cdot 8{,}3142 + 0{,}0133 \cdot T + 6{,}32 \cdot 10^{6} \cdot T^{-2}$	[18]
(6)	$La_{55}Al_{25}Cu_{10}Ni_{10}$	$\Delta C_p = 3{,}44 \cdot 10^{-2} \cdot T + 1{,}46 \cdot 10^{6} \cdot T^{-2} - 36{,}63 \cdot 10^{-6} \cdot T^{2}$	[4]
(7)	$La_{55}Al_{25}Cu_{10}Ni_5Co_5$	$\Delta C_p = 2{,}62 \cdot 10^{-2} \cdot T + 1{,}69 \cdot 10^{6} \cdot T^{-2} - 18{,}13 \cdot 10^{-6} \cdot T^{2}$	[4]
(8)	$La_{62}Al_{14}Cu_{20}Ag_4$	$C_p^{\,s} = 3 \cdot 8{,}3142 + (-0.00869) \cdot T + 3{,}04 \cdot 10^{-5} \cdot T^{2}$ $C_p^{\,l} = 3 \cdot 8{,}3142 + 0{,}024739 \cdot T + 7{,}54 \cdot 10^{5} \cdot T^{-2}$	[22]
(9)	$Cu_{47}Ti_{34}Zr_{11}Ni_8$	$C_p^{\,s} = 3 \cdot 8{,}3142 + (-0.00089) \cdot T + 6{,}82 \cdot 10^{-6} \cdot T^{2}$ $C_p^{\,l} = 3 \cdot 8{,}3142 + 0{,}0156 \cdot T + 2{,}83 \cdot 10^{6} \cdot T^{-2}$	[18]
(9)	$Cu_{47}Ti_{34}Zr_{11}Ni_8$	$C_p^{\,s} = 3 \cdot 8{,}3142 + (-0.0007882) \cdot T + 6{,}842 \cdot 10^{-6} \cdot T^{2}$ $C_p^{\,l} = 3 \cdot 8{,}3142 + 0{,}0154050 \cdot T + 3{,}4744 \cdot 10^{6} \cdot T^{-2}$	[13]
(10)	$Mg_{65}Cu_{25}Y_{10}$	$C_p^{\,s} = 3 \cdot 8{,}3142 + (-0{,}005651) \cdot T + 16{,}338 \cdot 10^{-6} \cdot T^{2}$ $C_p^{\,l} = 3 * 8{,}3142 + 0{,}0190070 \cdot T + 1{,}2264 \cdot 10^{6} \cdot T^{-2}$	[13]
(10)	$Mg_{65}Cu_{25}Y_{10}$	$C_p^{\,s} = 3 \cdot 8{,}3142 + (-0{,}0038) \cdot T + 1{,}02 \cdot 10^{-5} \cdot T^{2}$ $C_p^{\,l} = 3 \cdot 8{,}3142 + 0{,}0137 \cdot T + 1{,}80 \cdot 10^{6} \cdot T^{-2}$	[24]
(11)	$Pd_{40}Ni_{40}P_{20}$	$C_p^{\,s} = 3 \cdot 8{,}3142 + (-0.0007092) \cdot T + 4{,}4605 \cdot 10^{-6} \cdot T^{2}$ $C_p^{\,l} = 3 \cdot 8{,}3142 + 0{,}0143050 \cdot T + 4{,}1169 \cdot 10^{6} \cdot T^{-2}$	[13]
(12)	$Pd_{40}Ni_{10}Cu_{30}P_{20}$	$C_p^{\,s} = 3 \cdot 8{,}3142 + (-0.0097270) \cdot T + 26{,}704 \cdot 10^{-6} \cdot T^{2}$ $C_p^{\,l} = 3 \cdot 8{,}3142 + 0{,}0113450 \cdot T + 6{,}0421 \cdot 10^{6} \cdot T^{-2}$	[13]
(13)	$Pd_{43}Ni_{10}Cu_{27}P_{20}$	$C_p^{\,s} = 3 \cdot 8{,}3142 + (-0.00549) \cdot T + 18{,}948 \cdot 10^{-6} \cdot T^{2}$	[13]

(14)	$Pt_{57,3}Cu_{14,6}Ni_{5,3}P_{22,8}$	$C_p^{\,l} = 3 \cdot 8{,}3142 + 0{,}0118960 \cdot T + 5{,}091 \cdot 10^{6} \cdot T^{-2}$ $C_p^{\,s} = 3 \cdot 8{,}3142 + (-0.00193) \cdot T + 6{,}738 \cdot 10^{-6} \cdot T^{2}$	[13]
(14)	$Pt_{57,3}Cu_{14,6}Ni_{5,3}P_{22,8}$	$C_p^{\,l} = 3 \cdot 8{,}3142 + 0{,}0053340 \cdot T + 5{,}9730 \cdot 10^{6} \cdot T^{-2}$ $C_p^{\,s} = 3 \cdot 8{,}3142 + (-0{,}0044622) \cdot T + 0{,}000011977 \cdot T^{2}$	[26]
(15)	$Au_{81,4}Si_{18,6}$	$C_p^{\,l} = 3 \cdot 8{,}3142 + 0{,}0056268 \cdot T + 5764840 \cdot T^{-2}$ $\Delta C_p = 28{,}6186 - 53{,}7640 \cdot 10^{-3} \cdot T + 3{,}2949 \cdot 10^{-5} \cdot T^{2}$	[27]
(16)	$Au_{77}Ge_{13,6}Si_{9,4}$	$\Delta C_p = 32{,}5264 - 63{,}0822 \cdot 10^{-3} \cdot T + 3{,}4141 \cdot 10^{-5} \cdot T^{2} + 1{,}3004 \cdot 10^{-2} / T + 2{,}5188 \cdot 10^{-4} / T^{2}$	[27]
(17)	$Pd_{77,5}Cu_{6}Si_{16,5}$	$C_p^{\,s} = 19{,}10828 + 0{,}0119199 \cdot T$ $C_p^{\,l} = 3 \cdot 8{,}3142 + 0{,}0154568 \cdot T + 2382079{,}822 \cdot T^{-2}$	[25]

Tab. 2

	Materials	Refs.
1	GeO_2	[6, 8, 28, 38-39]
2	BeF_2	[6]
3	Methanol	[6, 40-41] [42]
4	n-propanol	[6,40, 41]
5	$ZnCl_2$	[6, 40, 44]
6	Butyronitrile	[6, 40]
7	Ethylene glycol	[6, 40, 43]
8	Ethanol	[6, 40, 43]
9	m-xylene	[6]

10	Glycerol	[6, 40, 43]
11	3-bromopentane	[6-7, 43]
12	m-cresol	[6]
13	2-methylpentane	[6, 19, 43]
14	β-D-fructose	[6, 43]
15	Phenolphthalein	[6, 40, 43]
16	Indomethacin	[6]
17	2-methyltetrahydrofuran	[6-7] [43]
18	Hydrochloro-thiazide	[6]
19	Griseofulvin	[6]
20	1,3,5-tri-α-naphthylbenzene	[6, 43]
21	Diethylphthalate	[6, 43]
22	Probucol	[6]
23	9-bromophenanthrene	[6]
24	Phenobarbital	[6]
25	D-glucose	[6, 40]
26	Maltitol	[6]
27	Glibenclamide	[6]
28	Salol	[6, 40, 43]
29	m-toluidine	[6, 40]
30	Flopropione	[6]

31	o-terphenyl	[6, 40, 43]
32	α-phenyl-cresol	[6]
33	Selenium	[6, 40, 43]
34	Triphenylethene	[6]
35	Sorbitol	[6, 40]
36	H_2SO_4-$3H_2O$	[6, 40]
37	Toluene	[6, 40, 43]
38	Sucrose	[6, 40]
39	Ca $(NO_3)_2$-$4H_2O$	[6, 40-41, 45]
40	Propylene carbonate	[6, 40, 42]
41	Triphenyl phosphite	[6, 40]
42	cis-/trans-decalin	[6]
43	As_2Te_3	[6]
44	B_2O_3	[6]
45	2-methyl-1-propanol	[6]
46	As_2Se_3	[6, 40]
47	m-fluorotoluene	[6]
48	Ethylbenzene	[6, 43]
49	3-methylpentane	[6]
50	n-butene	[6, 40]
51	Isopropylbenzene	[6]

52	Xylitol	[6]
53	PMS	[6, 40]
54	Li-acetate	[6, 40]
55	1-2 propandiol	[7, 40]
56	$CaAl_2Si_2O_8$	[7, 40]
57	SiO_2	[8, 28, 38, 46]